AMMT – 2004
National Conference on Advanced Materials and Manufacturing Techniques, March 08-09, 2004
JTNTU College of Engineering, Hyderabad and CITD, Hyderabad

ELASTIC RIGID-BODY DYNAMIC MODELING OF PLANAR PARALLEL ROBOT ACTUATED BY SERVOMOTORS

A. Chennakesava Reddy[1] and **P. Rami Reddy**[2]

[1]Associate Professor, Department of Mechanical Engineering
JNTU College of Engineering, Kukatpally, Hyderabad – 500 072

[2]Registrar, J. N. T University, Kukatpally, Hyderabad –500 072

ABSTRACT: This paper presents elastic rigid-body dynamic modeling of planar parallel robot using high reduction gears. The robot is redundantly actuated by three servomotors with high-reduction gears. The robot is equipped with structurally integrated torque sensors. The paper concludes that even though the gearboxes affect the dynamics but they are hardly backdriveable.

Keywords: *Elastic rigid body dynamic modeling, planar parallel robot, servomotors*

1. INTRODUCTION

Actuation redundancy occurs whenever a mechanism has more actuated joints than kinematic degrees of freedom. This happens only if at least one closed kinematic chain is formed. Actuation has been investigated for various mechanisms such as robot fingers, robot wrists, robot shoulders, and waking robots [1-9]. In all the cases direct or semi-direct (low gear reductions) were used. This allows output torque sensing using motor currents and a rigid body dynamic modeling [10]. Parallel robots are closed-chain robots. The actuators are fixed to close to a base, and connected to a traveling plate by kinematic chains. A very high-speed motion may result due to fixed actuators and lightweight design [11]. The parallel robots have limited workspace than serial robots and multi-degrees of freedom are necessary to allow spatial motion. Planar parallel robots move in the plane and need only one degree of freedom.

Automated pick-and-place tasks require fast robots with a reasonable workspace, medium payload, but high acceleration and velocity for efficiency. Four Cartesian degrees of freedom (i.e., x, y, z and 360^0 rotation about the z-axis) are sufficient. Fully parallel direct-drive robots can easily meet the requirements of acceleration and velocity. But, the rotation of end-effector is limited and the workspace is smaller than the size of the robot.

This paper focuses on the development of elastic rigid dynamic modeling of planar robot considering the effects of gearboxes on the torque.

2. PLANAR PARALLEL ROBOT

It is two degrees of freedom planar parallel robot with one additional leg, which introduces actuation redundancy [Fig.1]. The three actuators are placed in a mutual distance of 1000 mm. The robot has joints with ball bearings and lightweight aluminium tube links. All links have equal length, l = 488 mm. Epicyclic gears with a reduction ratio 80 are used for high stiffness and precision of the robot.

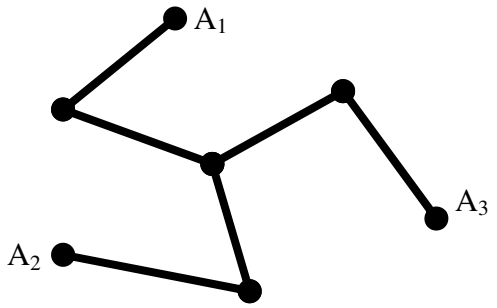

Fig.1 Planar parallel robot with three actuators

Tracking errors may cause transient antagonistic actuation during the movement of the robot. This may result in uncontrolled forces inside the robot structure causing wear or damage. The uncontrolled forces are proportional to the stiffness. Highly elastic links are used to reduce the forces [12]. The strain gauges are employed to pick up the internal forces and control them by feedback and redundant actuation.

3. ELASTIC RIGID - BODY MODELING

The generalized elastic and rigid-body coordinates are shown in Fig.2. The A_i denote the actuators, B_i are the unactuated joints with ball bearings and C is the end-effector. The origin of Cartesian reference frame is at A_1. Passive joints and links B,C are assumed to be rigid. The angles $\theta_{l,r}$ denote the active joint coordinates and $\theta_{l,e}$ represent the elastic coordinates of joint B_i.

The angular deflection is given by

$$\Delta\theta_i = \theta_{i,e} - \theta_{i,r} \qquad \ldots(1)$$

The angular deflection is proportional to the bending torque τ_l picked up by the strain gauges,

$$\Delta\theta_i = k_{T,l}\tau_l \qquad \ldots(2)$$

where $k_{T,l}$ are the torsional stiffness of the links.

It is known fact that k redundant actuators add k columns to the non-reduntant Jacobian

$$J_{nd}(\theta) = \frac{\partial x}{\partial \theta_{nd}} \qquad \ldots(3)$$

where $x - [x\ y]^T$ is the coordinate vector of the end-effector in the Cartesian reference frame and θ_{nd} denotes the vector of active joint coordinates.

The static force transmission of a non-redundant robot

$$f = \left[J_{nd}^{-1}\right]^T \tau_{nd} \qquad \ldots(4)$$

with F being the Cartesian force vector and τ_{nd} the vector of n actuator torques.

$$f = G\tau \qquad \ldots(5)$$

where, G = the n X (n+k) transposed inverse Jacobian and τ consists of (n+k) actuator torques.

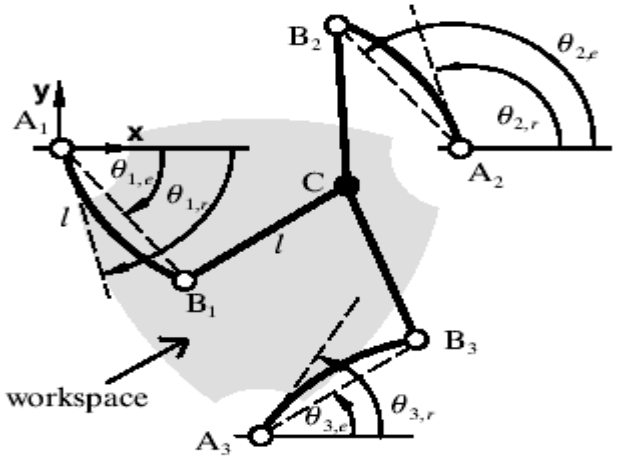

Fig.2 Elastic and rigid-body coordinates of the robot

The torque vector τ can be decomposed into the vector of torques with minimum 2-norm,

$$\tau_m = G^{-1} G\tau \qquad \ldots(6)$$

and torque vectors which belong to the null-space of G and produce zero output force,

$$\tau_k = (I - G^{-1} G)\ \tau \ldots(7)$$

τ_k allows the optimal scaling of torques, which produce only internal forces, which is the principle of redundant actuation.

Assuming linear springs

$$\Delta\theta = \frac{1}{k_{T,l}}\tau \qquad \ldots(8)$$

The small deflections of the links can be decomposed as mentioned in (1) caused by the actuator torques and reaction forces into those cause an elastic deflection at the end-effector.

$$\Delta\theta_m = \frac{1}{k_{T,l}} G^{-1} G \tau \qquad \ldots(9)$$

those do not cause

$$\Delta\theta_m = \frac{1}{k_{T,l}} \left(I - G^{-1}G\right)\tau \qquad \ldots(10)$$

the Cartesian elastic deflection

$$\Delta x = x_e - x_r \qquad \ldots(11)$$

where x_e is the actual elastic position and x_r is the virtual rigid position of the end-effector.

Using (3) and (8), the Cartesian deflection

$$\Delta x = J\Delta\theta_m = \frac{1}{k_{T,l}} G^{-1^T} G^{-1} \tau \qquad \ldots(12)$$

The elastic decomposition (10) and (12) for a given rigid position is shown in Fig.3. It can be seen that the oscillatory behavior of (c) differ greatly from (a) and (b), since the same spring constant $k_{T,l}$ is involved, but instead of the joint masses and playload oscillating against the elastic links, there is a rotary oscillation of the actuators. Since neither the position C of the end-effector nor the joint positions B_i are affected, the actuator torques act against cantilever beams with fixed end position B_i. As they act antagonistically in a way that the forces in the links B_iC cancel exactly, there is a perfect decoupling of all three actuators in this mode, and the oscillation does not vary with position of the end-effector neither in frequency nor damping. This type of oscillation occurs only in the null-space, since only torques τ_k and deflections $\Delta\theta_k$ are involved.

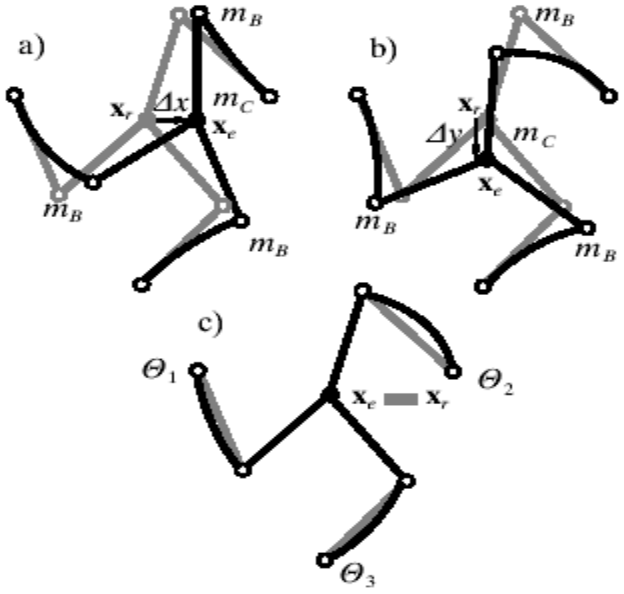

Fig.3 Elastic decomposition and principle modes of oscillations

4. EFFECT OF GEARBOXES

The presence of gearboxes is neglected till now. The stiffness of the gearboxes is in the same order of magnitude as the stiffness of the structure, and different friction effects that cause hysteresis affect the dynamics of the robot.

Fig.4 shows drive train I contributing to motion degrees of freedom. The gearbox is modeled as a linear torsional spring plus friction. F is the force acting along the inner link I caused by inertia and external forces at the end-effector C.

$K_{T,l}$ = 15000 Nm/rad
$K_{T,g}$ = 18375 Nm/rad
$n_g^2\theta_{motor} = 0.413\text{Kgm}^2$
$n_g^2\theta_g = 0.413\text{Kgm}^2$
$m_B l^2$ = 0.094 Kgm^2

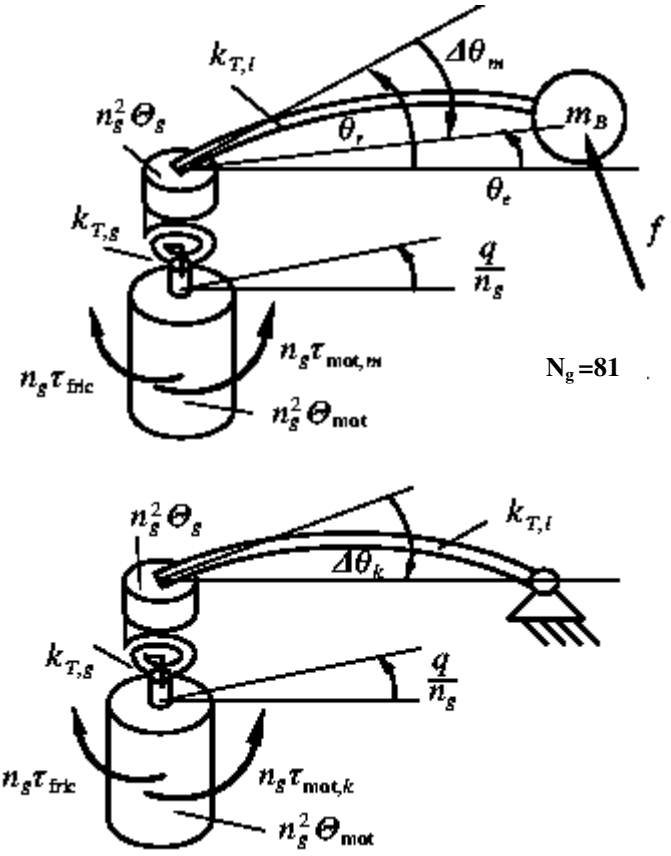

Fig.5. Drive train model in null-space

The null-space gives a different picture as shown in Fig.5. The moment of inertia of motor and gearbox are involved only. The unknown viscous friction is assumed to be concentrated at the gear input and the cantilever beam to be undamped.

The equations of motions of the drive train in Fig.5 are with d_g being a viscous friction coefficient with respect to the gear input.

$$\tau_{fri} = d_g \dot{q} \qquad \ldots(12)$$

$$n_z^2\theta_{motor}\frac{\ddot{q}}{n_g}+n_z^2\theta_g\frac{\dot{q}}{n_g}+k_{T,g}\left(\frac{q}{n_g}-\Delta\theta_k\right)=n_g\tau_{motor} \qquad \ldots(13)$$

$$n_g^2\theta_g\Delta\ddot{\theta}_k+\left(k_{T,l}+k_{T,g}\right)\Delta\theta_k=k_{T,k}\frac{q}{n_g} \qquad \ldots(14)$$

Now, using the fact that $\theta_g < \theta_{motor}$, the order of the system can be reduced from 4 to 2 by setting $\theta_g = 0$. Taking the Laplace transform of (13) and (14), eliminating q, and introducing the bending torque of the link.

$$\tau_{l,k}=k_{T,l}\Delta\theta_k \qquad \ldots(15)$$

The transform function from the motor torque to the torque in the cantilever beam is obtained

$$\frac{\tau_{l,k}}{\tau_{motor,k}}=\frac{n_g k_{T,l}k_{T,g}}{n_g^2\theta_{motor}\left(k_{T,l}+k_{T,g}\right)s^2+n_g^2 d_g\left(k_{T,l}+k_{T,g}\right)s+k_{T,l}k_{T,g}} \qquad \ldots(16)$$

The steady state gain is the gear ratio. The unknown friction constant d_g is found by matching the step response. One drive train with fixed joint B is excited with a motor torque reference step of –0.8 Nm. The response signal of the strain gauges is shown in Fig.6. For best matching d_g = 0.016 NmS/rad. The experimental steady state gain loss is caused by Coulomb friction worth 5 Nm. This is on account of d_g, which is the only parameter to model the gearbox friction effects, and also owing to very little rotation of the gears takes place. The equation becomes to a second order lag

$$\frac{\tau_{l,k}}{\tau_{motor,k}}=\frac{81}{5.249x10^{-5}s^2+0.031s+1} \qquad \ldots(17)$$

with undamped natural frequency ω_n = 138 s^{-1} and damping ratio = 0.9.

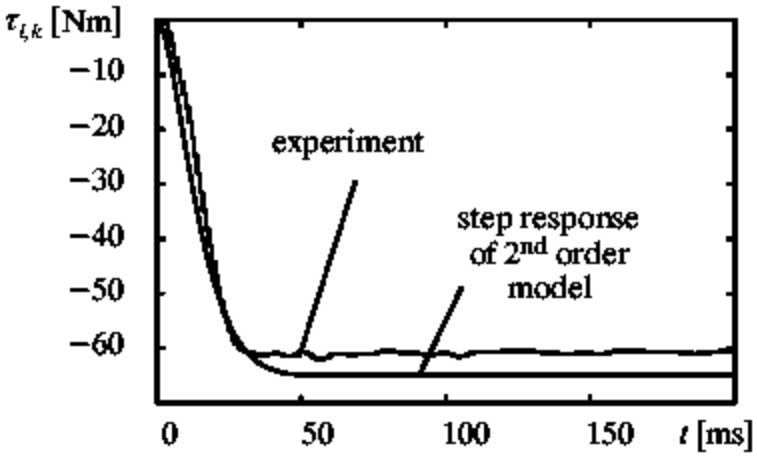

Fig.6 Step response of the drive train with fixed joint B and motor torque = 0.8 Nm

5. RIGID-BODY MOTION

All links are assumed to have zero mass, all other masses involved are lumped in the actuator moments of inertia $\Theta=n_g^2\left(\Theta_{motor}+\Theta_g\right)+m_B l^2=0.55Kgm^2$, and concentrated mass of the center joint m_c = 0.5 Kg. A gearbox friction coefficient d_g = 0.002 NmS/rad for fast motion is calculated from measuring motor currents with the gearbox attached at constant rates.

The sum of Cartesian inertial and external forces acting on joint C

$$m_c\ddot{x}+f_{external} \qquad \ldots(18)$$

are mapped onto joint torque by G^{-1}, so that the equations of motion for actuators become

$$\Theta\ddot{\theta} + n_g^2 d_g \dot{\theta} + G^{-1}\left(m_c \ddot{x} + f_{external}\right) = n_g \tau_{motor,m} \qquad \ldots(19)$$

$\theta = \frac{1}{n_g}[q_1, q_2, q_3]^T$ is the coordinate vector of absolute encoder readings transformed into robot joint coordinates.

No gravity forces are present in horizontal operation. Using

$$\dot{\theta} = G^T \dot{x}, \quad \ddot{\theta} = \dot{G}^T \dot{x} + G^T \ddot{x} \text{ and } GG^{-1} = \mathrm{I}$$

and multiplying from the left with G, the Cartesian equations of motion are obtained.

$$M\ddot{x} + \dot{x} = n_g G \tau_{motor} - f_{exteral} \qquad \ldots(20)$$

The motor torque components in the null-space of g do not contribute to motion.

$$G\tau_{motor,m} = G\tau_{motor} \qquad \ldots(21)$$

$$M = \Theta GG^{-1} + \begin{bmatrix} m_c & 0 \\ 0 & m_c \end{bmatrix} \qquad \ldots(22)$$

is the Cartesian mass matrix and

$$C = n_g^2 d_g GG^T + \Theta GG^T \qquad \ldots(23)$$

contains Cartesian centrifugal, Coriolis and viscous friction components.

6. EXPERIMENTAL VERIFICATION

The Cartesian model was verified after the robot control system and a null-space feedback controller were set up. Tracking a reference trajectory (a 250 mm equilateral triangle) with 50 m/s^2 acceleration and 3 m/s velocity, the measured current reference of motor-1 was compared with the calculated current

$$i - \frac{k_0}{n_g}\left(M\ddot{x}_{reference} + C\dot{x}_{reference}\right) \qquad \ldots(24)$$

where k_0 is the current to torque ratio of the motor.

The total calculated current is decomposed into components of inertia, friction and centrifugal and Coriolis forces and torques according to (22) and (23). The total computed current is approximately equal to the experimental current.

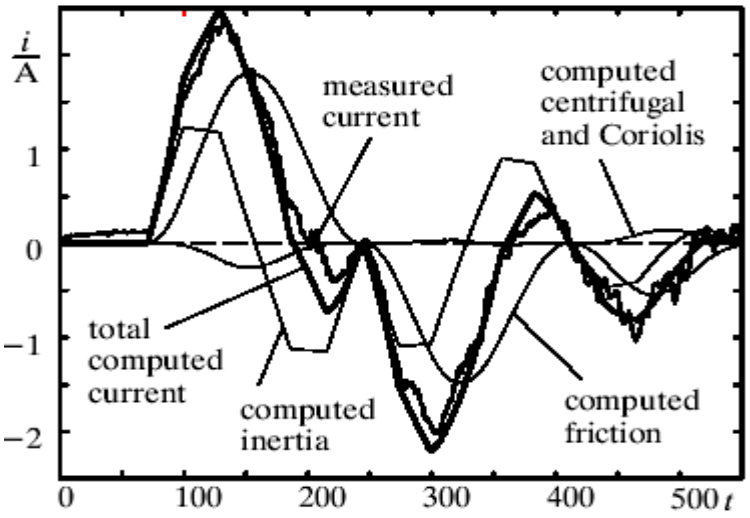

Fig.7 Verification of computed current with experimental current

7. CONCLUSIONS

This paper presents two decoupled dynamic models for the motion and the null-space of two degrees of freedom parallel manipulator with one redundant actuator. The strain gauges are employed to pick up the internal forces and control them by feedback and redundant actuation. This allows setting up separate control loops for the motion and for the torque degrees of freedom. It is found that the gearboxes influence very little on dynamics and are hardly backdriveable. The total calculated current is decomposed into components of inertia, friction and centrifugal and Coriolis forces and torques. The total computed current is approximately equal to the experimental current.

References

1. A. Chennakesava Reddy, Robot and its engineering field applications, Journal of Engineering Advances, 0971-2968, vol.14, no.01, pp.33-35, (2002).
2. B. Rajasekhara Reddy, A. Chennakesava Reddy, Obstacle avoidance of planar redundant manipulators for pick-and-place operations using real-coded genetic algorithm, National Conference on Advances in Manufacturing Technology, Palghat, 15-16th February, 5-A-2, (2003).
3. A. Chennakesava Reddy, B. Kotiveerachari, P. Ram Reddy, Kinematic model of a flexible link using local curvatures as the deformation coordinates, National Conference on Advances in Manufacturing Technology, Palghat, 15-16th February, 1-A-7, (2003).
4. B. Rajasekhara Reddy, A. Chennakesava Reddy, Dynamic modeling of two-link robot arm driven by DC motors using linear graph theory and principles of mechanics, National Conference on Trends in Mechanical Engineering, Warangal, 30th August, pp.130-132, (2003).
5. A. Chennakesava Reddy, P. Ram Reddy, B. Kotiveerachari, Two methods for computing reduced-form dynamics of closed – chain mechanism, National Conference on Trends in Mechanical Engineering, Warangal, 30th August, pp.133-136, (2003).
6. B. Kotiveerachari, A. Chennakesava Reddy, Kinematic and static analysis of gripper fingers using reciprocal screws, National Conference on Computer integrated Design and Manufacturing, Coimbatore , 28-29th November, pp.121-124,(2003).
7. A. Chennakesava Reddy, P. Ram Reddy, Hazard detection for multi - agent reactive robotic system using on - line software analysis of safety constraints, National Conference on Computer integrated Design and Manufacturing, Coimbatore , 28-29th November, pp.294-301, (2003).
8. A. Chennakesava Reddy, B. Kotiveerachari, P. Ram Reddy, Finite element analysis of flexibility in mobile robotic manipulators, Journal of Institution of Engineers, 0257-6708, v.85, n.02, pp.27-31, (2004).
9. Kurtz.R, Hayward.V, Multiple-goal kinematic optimization of a spherical mechanism with actuator redundancy, IEEE Transactions on Robotics and Automation, Vol.8, No.5, p.644.651, (1992).
10. Nahon. M.A, Angeles. J, Force optimization in redundantly actuated closed kinematic chains, IEEE International Conference on Robotics and Automation, Scottsdale, AZ, pp.951-956, (1995).
11. Reiner. I, Redundant actuation of a closed-chain manipulator, Advanced Robotics, Vol.11, No.3, pp.233-245, (1997)
12. Nakamura. Y, Ghodoussi. M, Dynamics computation of closed-link robot mechanisms with nonredundant and redundant actuators, IEEE Transactions on Robotics and Automation, Vol.5, No.3, pp.294-302, (1989).